

Lewis acid-doped transition metal dichalcogenides for ultraviolet-visible photodetectors

Heng Yang(杨恒), Mingjun Ma(马明军), Yongfeng Pei(裴永峰), Yufan Kang(康雨凡), Jialu Yan(延嘉璐), Dong He(贺栋), Changzhong Jiang(蒋昌忠), Wenqing Li(李文庆), and Xiangheng Xiao(肖湘衡)

Citation: Chin. Phys. B, 2024, 33 (**9**): 098501. DOI: 10.1088/1674-1056/ad597f
Journal homepage: http://cpb.iphy.ac.cn; http://iopscience.iop.org/cpb

What follows is a list of articles you may be interested in

A field-effect WSe_2/Si heterojunction diode

Rui Yu(余睿), Zhe Sheng(盛喆), Wennan Hu(胡文楠), Yue Wang(王越), Jianguo Dong(董建国), Haoran Sun(孙浩然), Zengguang Cheng(程增光), and Zengxing Zhang(张增星)
Chin. Phys. B, 2023, 32 (**1**): 018505. DOI: 10.1088/1674-1056/ac9049

A self-driven photodetector based on a SnS_2/WS_2 van der Waals heterojunction with an Al_2O_3 capping layer

Hsiang-Chun Wang(王祥骏), Yuheng Lin(林钰恒), Xiao Liu(刘潇), Xuanhua Deng(邓煊华),Jianwei Ben(贲建伟), Wenjie Yu(俞文杰), Deliang Zhu(朱德亮), and Xinke Liu(刘新科)
Chin. Phys. B, 2023, 32 (**1**): 018504. DOI: 10.1088/1674-1056/ac6dbd

New DDSCR structure with high holding voltage for robust ESD applications

Zi-Jie Zhou(周子杰), Xiang-Liang Jin(金湘亮), Yang Wang(汪洋), and Peng Dong(董鹏)
Chin. Phys. B, 2021, 30 (**3**): 038501. DOI: 10.1088/1674-1056/abd38f

Photodetectors based on junctions of two-dimensional transition metal dichalcogenides

Xia Wei(魏侠), Fa-Guang Yan(闫法光), Chao Shen(申超), Quan-Shan Lv(吕全山), Kai-You Wang(王开友)
Chin. Phys. B, 2017, 26 (**3**): 038504. DOI: 10.1088/1674-1056/26/3/038504

Field-effect transistors based on two-dimensional materials for logic applications

Wang Xin-Ran (王欣然), Shi Yi (施毅), Zhang Rong (张荣)
Chin. Phys. B, 2013, 22 (**9**): 098505. DOI: 10.1088/1674-1056/22/9/098505

Lewis acid-doped transition metal dichalcogenides for ultraviolet–visible photodetectors

Heng Yang(杨恒)[1], Mingjun Ma(马明军)[1], Yongfeng Pei(裴永峰)[1], Yufan Kang(康雨凡)[1], Jialu Yan(延嘉璐)[1], Dong He(贺栋)[1], Changzhong Jiang(蒋昌忠)[1], Wenqing Li(李文庆)[1,†], and Xiangheng Xiao(肖湘衡)[1,2,‡]

[1] *School of Physics and Technology, Key Laboratory of Artificial Micro- and Nano-Structures of Ministry of Education, Wuhan University, Wuhan* 430072, *China*

[2] *Wuhan Research Center for Infectious Diseases and Cancer, Chinese Academy of Medical Sciences, Wuhan* 430072, *China*

(Received 17 April 2024; revised manuscript received 8 June 2024; accepted manuscript online 19 June 2024)

Ultraviolet photodetectors (UV PDs) are widely used in civilian, scientific, and military fields due to their high sensitivity and low false alarm rates. We present a temperature-dependent Lewis acid p-type doping method for transition metal dichalcogenides (TMDs), which can effectively be used to extend the optical response range. The p-type doping based on surface charge transfer involves the chemical adsorption of the Lewis acid $SnCl_4$ as a light absorption layer on the surface of WS_2, significantly enhancing its UV photodetection performance. Under 365 nm laser irradiation, WS_2 PDs exhibit response speed of 24 ms/20 ms, responsivity of 660 mA/W, detectivity of 3.3×10^{11} Jones, and external quantum efficiency of 226%. Moreover, we successfully apply this doping method to other TMDs materials (such as MoS_2, $MoSe_2$, and WSe_2) and fabricate WS_2 lateral p–n heterojunction PDs.

Keywords: two-dimensional (2D) materials, p-type doping, transition metal dichalcogenides, photodetectors

PACS: 85.60.Gz, 85.60.Dw, 85.30.Tv **DOI:** 10.1088/1674-1056/ad597f

1. Introduction

Ultraviolet photodetectors (UV PDs) are widely used in civilian, scientific, and military fields due to their high sensitivity and low false alarm rate,[1] such as flame detection, ozone monitoring, biomedical detection, sterilization testing, missile warning, and ultraviolet communication.[2–4] Currently, the materials used for UV PDs are primarily silicon-based and wide bandgap semiconductor materials.[5–7] However, the integration requirements of Moore's law pose a significant challenge for devices based on traditional silicon materials, which encounter difficulties in size miniaturization. Meanwhile, it is difficult for most wide bandgap semiconductor materials to integrate with existing CMOS technology, and the growth process is complex and costly.[8,9] Therefore, finding new materials for UV PDs has become a research hotspot.

Two-dimensional (2D) transition metal dichalcogenides (TMDs) have exhibited great potential in the field of optoelectronic devices due to their continuously tunable bandgap and the dangling bond free surface.[10,11] Nevertheless, 2D TMDs face a significant challenge due to their inherent nature as narrow bandgap semiconductors, with typical bandgaps ranging from 1 eV to 2 eV.[12] This characteristic renders them responsive to visible and infrared light, yet unresponsive to the ultraviolet (UV) spectrum,[13] which severely limits the development of 2D TMDs materials in the field of ultraviolet photodetection.

Doping modification of semiconductor materials can regulate the light absorption range by manipulating the band structure.[14,15] Currently, doping methods for two-dimensional materials mainly include substitutional doping,[16,17] defect doping,[18,19] and surface charge transfer doping.[20,21] Surface charge transfer doping is widely utilized for its advantages of simple operation, no damage to the crystal structure, and the adjustable doping effect.[20]

In this study, we achieve the conversion of WS_2 from an n-type to a p-type semiconductor through surface charge transfer doping with an ethanolic solution of the Lewis acid $SnCl_4$. After doping with $SnCl_4$, the optical response range of WS_2 is extended from the visible to the ultraviolet–visible spectrum. This approach is also applicable to other 2D TMDs materials such as MoS_2, $MoSe_2$, and WSe_2, thereby creating new opportunities for applications of 2D TMDs in the field of ultraviolet photodetection.

2. Experimental details

Device fabrication To prepare few-layer WS_2 nanoflakes, a small piece of WS_2 crystal (HQ Graphene in the Netherlands) was repeatedly folded onto 3M tape using the mechanical exfoliation method. The nanoflakes were first pressed and transferred onto a PDMS substrate (Guijun Xin Material Technology Co., Ltd. in Hangzhou) and then transferred onto a 300 nm SiO_2/Si substrate (MAX Scientific and Industrial Co., Ltd). Electrode patterns were designed using Design CAD LT software, and the electrodes were patterned

†Corresponding author. E-mail: wenqing_li@whu.edu.cn
‡Corresponding author. E-mail: xxh@whu.edu.cn

© 2024 Chinese Physical Society and IOP Publishing Ltd

using an e-beam lithography system (JSM-6510). Finally, a vacuum evaporation coater (JSD-300) was used to deposit 15 nm of Cr and 50 nm of Au (Shanghai Aladdin Biochemical Technology Co., Ltd) as source-drain electrodes.

Doping treatment An appropriate volume of liquid anhydrous $SnCl_4$ (purity $\geqslant$ 99%, Thermo Fesel Technology Co., LTD.) was measured into 10 ml anhydrous ethanol solution (purity $\geqslant$99.5%, Sinopod Chemical Reagents Co., LTD.), and ultrasonic treatment for 10 min promoted the repeated dissolution to prepare an ethanol solution of $SnCl_4$. Under suitable temperature conditions, the prepared WS_2 FET was soaked in $SnCl_4$ ethanol solution for an appropriate time to carry out doping process. After treatment, the sample was washed with ethanol to remove the residual $SnCl_4$ on the surface, and the sample was blown dry with nitrogen (N_2) to ensure that there was no residual solvent on the surface.

Structure characterization Raman spectra and PL spectra were carried out by a confocal raman spectrometer (LabRAM HR Evolution of HORIBA) with a 532 nm laser in an atmospheric environment. Atomic force microscopy (AFM, Bruker, Dimension icon) was employed to analyze variations in the thickness and roughness of WS_2. The element composition and variations in the valence band spectrum of WS_2 surface was characterized by x-ray photoelectron spectroscopy (XPS, Escalab Xi+). The light absorption of $SnCl_4$ ethanol solution was measured by an ultraviolet visible absorption spectrometer (UV-2500).

Device measurements The probe station (Lake Shore CRYOTRONICS) and the semiconductor device analyzer (Keysight B1500A) were employed to investigate the electrical properties at room temperature in a vacuum environment. In the testing of optoelectronic properties, lasers at wavelengths of 500 nm, 600 nm, 700 nm, and 800 nm are provided by supercontinuum white light laser (SuperK EVO of NKT Photonics), while a laser at 365 nm is supplied by a portable ultraviolet analyzer (ZF-7A), and a high-precision electronic timer (GCI-73) used for assisting in the physical chopping of the 365 nm laser.

3. Results and discussion

The doping operation and structure schematics are shown in Figs. 1(a) and 1(b). The Raman spectrum was used to characterize the WS_2 before and after doping. The pristine WS_2 shows E_{2g} and A_{1g} mode of WS_2 at 351.86 cm^{-1} and 419.48 cm^{-1}, respectively,[22] as shown in Fig. 1(c). Minimal changes were observed in the Raman characteristic peaks of WS_2 after doping, indicating that the crystal structure remained intact without any destruction.

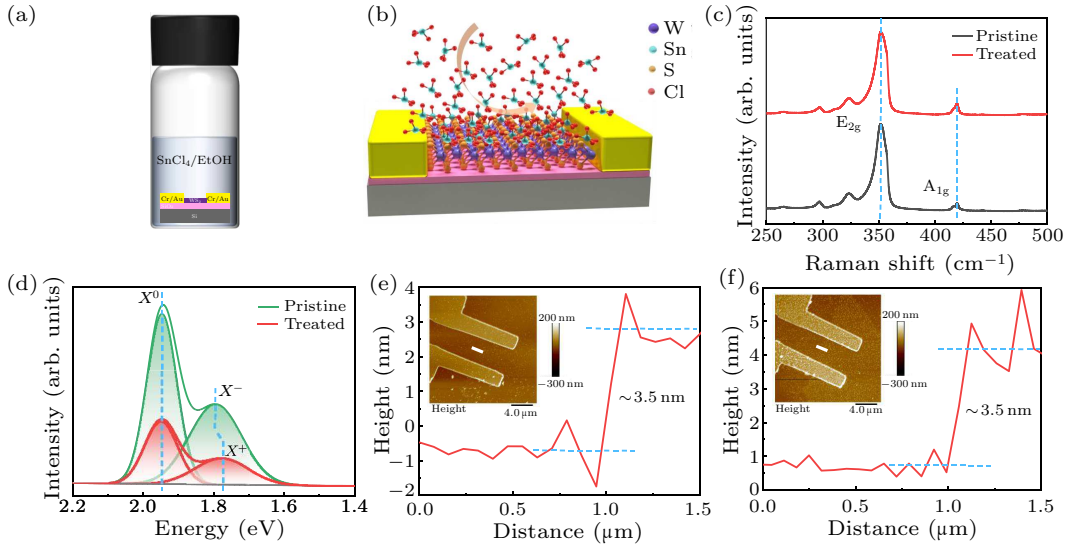


Fig. 1. (a) Schematic of WS_2 doping in the ethanolic solution of $SnCl_4$. (b) Structural schematic of $SnCl_4$ doped device. (c) Raman spectra and (d) PL spectra of WS_2 before and after doping in the Lewis acid $SnCl_4$ ethanol solution. Height distribution of WS_2 nanoplates (e) before doping and (f) after doping in the Lewis acid $SnCl_4$ ethanol solution, with insets showing their respective AFM images.

Subsequently, we analyzed the photoluminescence (PL) spectrum of WS_2 before and after doping. As shown in Fig. 1(d), the primary emission peak of WS_2 was located at 1.94 eV, which corresponded to the neutral exciton (X^0) emission peak resulting from the recombination of intrinsic carriers in WS_2.[23,24] Before doping, the emission peak at 1.79 eV was attributed to the electron-bound exciton (X^-) emission, which originated from the electron doping provided by the inherent S vacancies in WS_2.[24] After doping, the X^- emission peak shifted towards a lower energy by approximately 0.02 eV. This suggests that the doped Lewis acid Sn acted as an acceptor, introducing numerous holes that recombined with electrons from the S vacancies. Excess holes combined with excitons to form lower energy hole-bound excitons (X^+). Furthermore, it was observed that the intensity of the PL peak was significantly suppressed after doping. This was attributed to the in-

troduction of excessive holes during the charge transfer doping process, which inhibited radiative recombination and consequently reduced the fluorescence emission efficiency.[25,26]

An atomic force microscope (AFM) was used to characterize the morphology and thickness alterations of WS_2 before and after doping. The height distribution images in Figs. 1(e) and 1(f) show that the original WS_2 had a thickness of approximately 3.5 nm, which corresponds to roughly five atomic layers.[26] This indicates that the WS_2 nanoflakes obtained via mechanical exfoliation were few-layer structures. After doping, there was no significant change in the thickness of WS_2. The AFM images in the inset display the roughness average (R_a) of the pristine WS_2 as 3.78 nm, which increased to 12.52 nm after doping. This increase is believed to be caused by the adsorption of the dopant $SnCl_4$ onto the surface of WS_2, which enhances surface roughness.

Temperature is a crucial factor that affects the extent of surface charge transfer doping. To examine the temperature dependency of the doping effect, we conducted doping treatments under two different conditions: at 5 ℃ and at 70 ℃. The selection of 70 ℃ was made because the boiling point of the solvent ethanol is 78.37 ℃. The temperature was set to 70 ℃ to maximize the impact of temperature on the doping effects while preventing the boiling of the solvent, which could potentially interfere with the doping process.

X-ray photoelectron spectroscopy (XPS) was employed to characterize the samples with different-temperature doping. Figures 2(a) and 2(b) show the S 2p and W 4f core level spectra of WS_2 before and after doping, respectively. Distinct double peaks corresponding to S and W were clearly observed in the pristine WS_2 sample. The S 2p peaks were located at 164.1 eV ($2p_{1/2}$) and 162.9 eV ($2p_{3/2}$), while the W 4f peaks appeared at 35.4 eV ($4f_{5/2}$) and 33.3 eV ($4f_{7/2}$), respectively. These peak positions are consistent with those previously reported for WS_2.[27] Compared to the pristine WS_2, the S and W core level peaks of the doped WS_2 shifted towards lower binding energy, aligning with previous reports on XPS changes following p-type doping in 2D TMDs.[28] Additionally, as doping temperature increased, there was a shift towards lower binding energies in both S and W core energy levels. This indicates that increasing the doping temperature can effectively promote surface charge transfer and enhance the effectiveness of doping treatment.

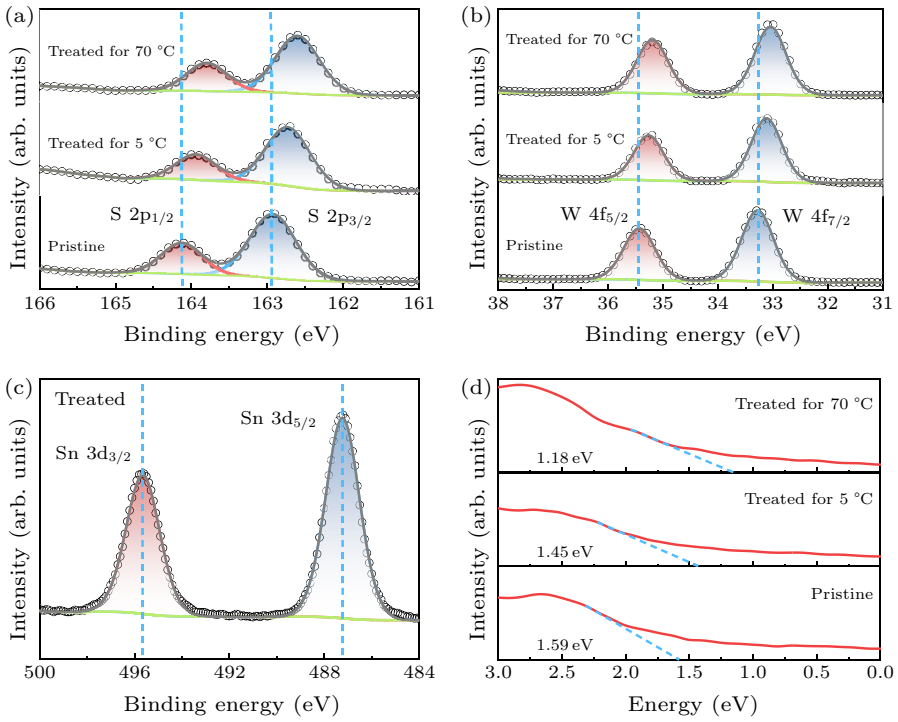


Fig. 2. (a) S 2p and (b) W 4f core-level binding energy spectra of WS_2 before and after doping in the Lewis acid $SnCl_4$ ethanol solution at 5 ℃ and 70 ℃. (c) Sn 3d core-level binding energy spectra of WS_2 after doping in the Lewis acid $SnCl_4$ ethanol solution at 70 ℃. (d) Valence band spectra of WS_2 before and after doping in the Lewis acid $SnCl_4$ ethanol solution at 5 ℃ and 70 ℃.

Additionally, the doped WS_2 sample showed the presence of Sn characteristic double peaks in Fig. 2(c), located at 495.6 eV ($3d_{3/2}$) and 487.2 eV ($3d_{5/2}$).[29] However, these characteristic peaks of Sn were absent in the pristine WS_2, indicating the presence of Sn^{4+} on the surface of WS_2 after doping. This suggested successful adsorption of $SnCl_4$ onto the surface of WS_2 during soaking treatment. Furthermore, Fig. 2(d) illustrates the valence band spectrum of WS_2 before and after doping. To find the energy difference between the valence band top and the Fermi level, we extrapolated the linear portion of the drawn curves near 0 eV until they intersect with a horizontal line. The point of intersection represented

the position of the valence band top relative to the Fermi level, denoted as E_v. As shown in Fig. 2(d), the E_v value for the pristine WS_2 is 1.59 eV. This value shifted to 1.45 eV after doping at 5 ℃ and further to 1.18 eV with increasing temperature. This result confirmed that Sn doping belonged to p-type doping and brought the Fermi level closer to the top of the valence band.

Characterization methods such as Raman, PL, AFM, and XPS were used to demonstrate that p-type doping based on surface charge transfer can be achieved in WS_2 through simple immersion in the ethanolic solution of the Lewis acid $SnCl_4$. This method is relatively ideal for dopant incorporation due to its simplicity and non-destructive nature.

Furthermore, we investigated the impact of doping treatment with the Lewis acid $SnCl_4$ on the electrical properties of WS_2 FETs. Figure 3(a) illustrates the transfer characteristic curves of WS_2 FETs before and after doping at temperature of 5 ℃. For the pristine WS_2 FET, the device exhibited n-type semiconductor behavior dominated by electron conduction. After doping, the device displayed ambipolar semiconductor behavior, indicating that Sn doping suppressed the n-type semiconductor behavior of WS_2. Figure 3(b) presents the transfer characteristic curves of the WS_2 doped at 70 ℃. The WS_2 FET displayed significant p-type semiconductor behavior dominated by hole conduction. The Lewis acid $SnCl_4$, acting as a receptor, can introduce holes into WS_2 during the doping process, thereby causing the Fermi level of WS_2 to approach the top of the valence band, as shown in Fig. 3(c). The increase in temperature provides the necessary activation energy for the chemical adsorption of $SnCl_4$, allowing more $SnCl_4$ to adsorb onto the surface of WS_2. This promotes the transfer of surface charges, introducing more holes into WS_2, leading to a further shift of the Fermi level closer to the top of the valence band, as shown in Fig. 3(d). As the temperature increases, WS_2 transforms from an n-type semiconductor to a bipolar and eventually a p-type semiconductor. This is consistent with the changes observed in the valence band spectrum of XPS analysis. Figures 3(e) and 3(f) depict the output characteristic curves of WS_2 FET before and after doping at 70 ℃. For the pristine WS_2 FET, the maximum source-drain current occurred at zero gate voltage. After doping, the maximum source-drain current was achieved at −60 V gate voltage. This change indicated that the doping effectively modulated the electrical conductivity and the doped WS_2 became a p-type semiconductor.

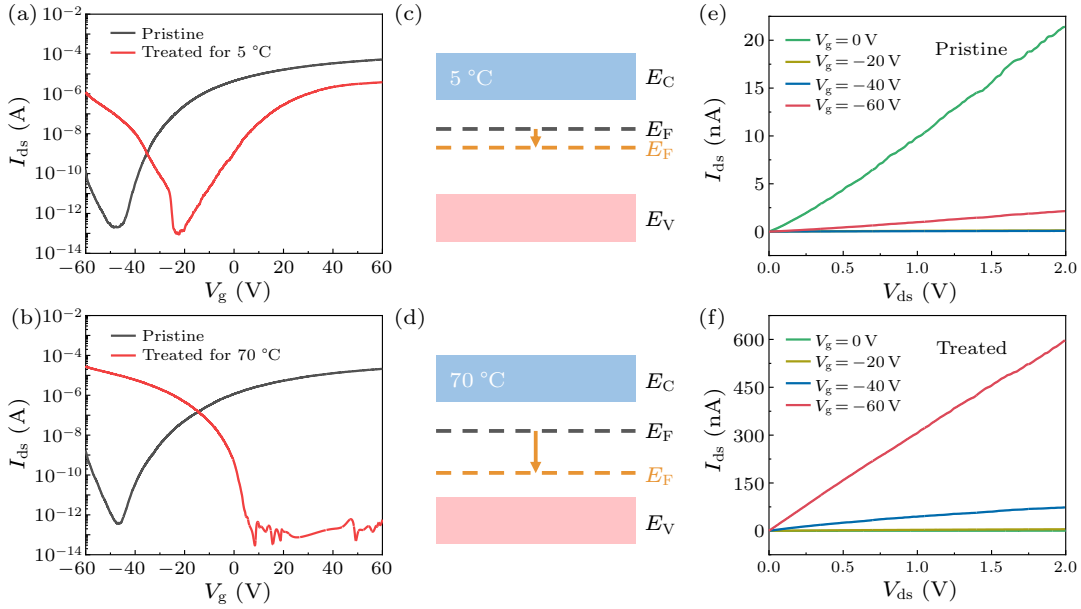


Fig. 3. Transfer characteristics of WS_2 FET before and after doping in the Lewis acid $SnCl_4$ ethanol solution at different temperatures: (a) 5 ℃ and (b) 70 ℃, with $V_{ds} = 1$ V. The schematics of the change of the band structure after doping at (c) 5 ℃ and (d) 70 ℃. Output characteristics of WS_2 FET at 70 ℃ (e) before and (f) after doping in the Lewis acid $SnCl_4$ ethanol solution, with V_g stepped from 0 V to −60 V in increments of −20 V.

In addition, we investigated the transfer characteristics of the devices with different doping concentrations and doping time gradients at 70 ℃, as shown in Fig. S1 of the supporting information. The results demonstrated that the doping level can be controlled by regulating the doping concentration and time parameters. Thus, precise doping of WS_2 can be achieved by adjusting the temperature, concentration, and time. To verify the effectiveness of the doping method, we doped nine devices, as shown in Fig. S2 of the supporting information. The consistent manifestation of pronounced p-type doping across all nine devices provides compelling evidence that this doping technique is robust and replicable.

Moreover, we have extended our research to the universality of Lewis acid p-type doping on TMDs. The doping of

MoS_2, $MoSe_2$, and WSe_2, which are commonly studied in TMDs, with Lewis acid was also carried out. As shown in Fig. S3, significant p-type doping effects were observed after doping, indicating that Lewis acid $SnCl_4$ has a certain degree of universality for TMDs.

To further investigate the effects of Sn doping on WS_2 FETs, the photoelectric properties of WS_2 FETs before and after doping were also tested and studied. Figures 4(a) and 4(b) show the output characteristics of WS_2 PDs before and after doping under laser illumination at different wavelengths. Both doped and undoped WS_2 PDs exhibited good optical response properties in the visible range of 500–800 nm. Notably, the pristine WS_2 PDs did not exhibit obvious optical switching behavior, as shown in Fig. S4. Figure 4(c) demonstrates the photoelectric current response of WS_2 PDs with doping treatment under pulsed laser irradiation at various wavelengths. Notably, the laser (SuperK EVO) available for our experiment could only provide continuous laser emission within the 500–900 nm range, hence the 365 nm laser used here was supplied by a portable UV analyzer (ZF-7A). During the measurement of the photoelectric current response, an additional high-precision electronic timer (GCI-73) was introduced to perform physical chopping. The small aperture size of the electronic timer's light path limited the incident fluence of the 365 nm laser, resulting in a reduced response current. As shown in Fig. 4(d), Sn doping significantly enhanced the optical response at 365 nm and provided rapidly optical switching speed. The photocurrent $I_{\text{illumination}}$ is 10.5 pA, and the dark current I_{dark} is 2 pA, calculating a net photocurrent I_{ph} as 8.5 pA. The rise time (T_{rise}) and fall time (T_{fall}) were measured to be 24 ms and 20 ms, respectively, where T_{rise} is defined as the time for $I_{\text{illumination}}$ to rise from 10% to 90%, and T_{fall} is the time for $I_{\text{illumination}}$ to decrease from 90% to 10%.

Furthermore, we also calculated the optical response speed T_{rise} and T_{fall} of WS_2 PDs before and after doping under 600 nm laser illumination, as shown in Fig. S5. A comparison revealed that Sn doped WS_2 PDs had faster optical switching speeds. This suggests that Sn doping not only significantly enhanced the photoelectric performance in the ultraviolet region but also improved in the visible region.

To comprehensively evaluate the photodetection performance of Sn doped WS_2 PDs in the UV region, we calculated the key performance parameters of WS_2 the photodetectors, including the responsivity (R), the specific detectivity (D^*), and the external quantum efficiency (EQE).

The responsivity (R) is an indicator of the PDs' ability to convert optical signals into electrical signals and is calculated by the formula

$$R = \frac{I_{\text{ph}}}{P_\lambda S}, \tag{1}$$

where P_λ is the incident light power (0.08 mW/cm^2) and S is the effective illumination area (16 μm^2), calculating the R is 664 mA/W.

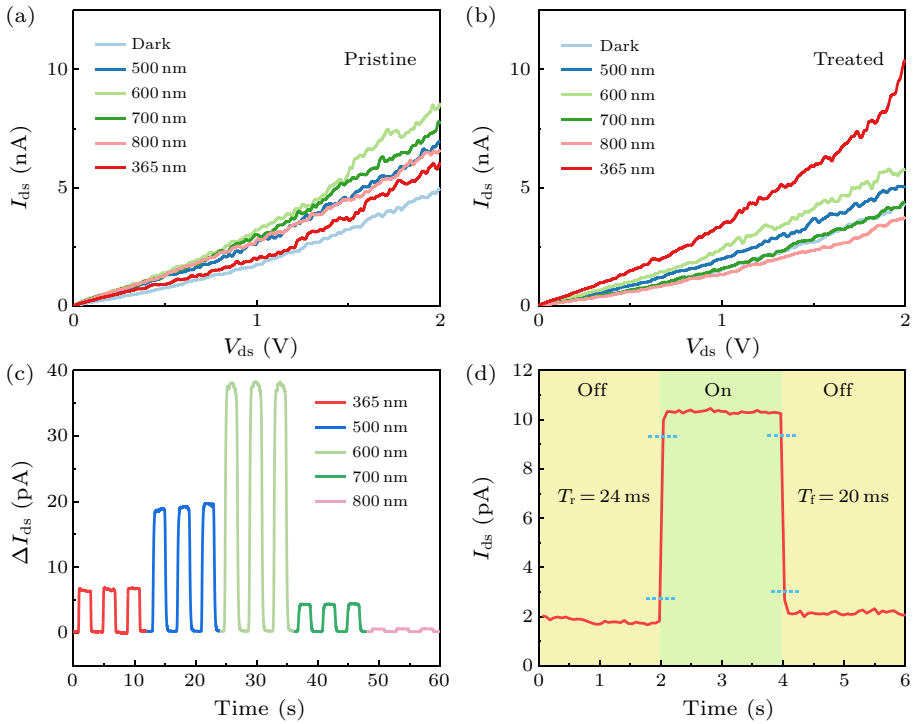


Fig. 4. Output characteristics of WS_2 PDs in dark and under various wavelength laser irradiation (a) before and (b) after doping in the Lewis acid $SnCl_4$ ethanol solution. Power densities for different wavelengths of lasers are as follows: 500 nm (0.65 mW/cm^2), 600 nm (2.6 mW/cm^2), 700 nm (1.15 mW/cm^2), 800 nm (2.05 mW/cm^2), 365 nm (0.08 mW/cm^2). (c) Photoresponse of doped WS_2 PDs at different laser wavelengths, with $V_{ds} = 0.1$ V. (d) Photoresponse switching speed of doped WS_2 PDs at 365 nm laser irradiation, with $V_{ds} = 0.1$ V.

The specific detectivity (D^*) is a parameter describing the PDs' capability to detect weak light signals under specific conditions and is calculated by the formula

$$D^* = R\sqrt{\frac{S}{2eI_{\text{dark}}}}, \tag{2}$$

where e is the electron charge (1.6×10^{-19} C), and D^* is calculated to be 3.32×10^{11} Jones.

The EQE is a parameter describing the efficiency of the PDs in converting incident photons into output current and is calculated by the formula

$$\text{EQE} = R\frac{hc}{e\lambda} \times 100\%, \tag{3}$$

where h is Planck's constant (6.626×10^{-34} J·s), c is the speed of light in vacuum (3×10^8 m/s), λ is the incident laser wavelength (365 nm), the calculated EQE is 226%.

The given key performance parameters demonstrate that Sn-doped WS_2 PDs exhibit exceptional photoelectric performance in the ultraviolet region, surpassing or comparable to other photodetectors based on transition metal dichalcogenides (TMDs), as shown in Table 1.

To investigate the mechanism by which Lewis acid $SnCl_4$ doping enhances the photoelectric performance of WS_2 PDs, we measured the UV-vis absorption spectrum of a $SnCl_4$ ethanol solution using anhydrous ethanol as a baseline (detailed in Fig. S6). The results show strong optical absorption by the $SnCl_4$ ethanol solution at around 365 nm, which is consistent with the significant enhancement of UV photoresponse observed in Sn-doped WS_2 PDs at the same wavelength. This result is in agreement with the previous reports on utilizing optical absorption layers to improve the photoresponse of PDs.[37] This indicates that when Sn was adsorbed onto the surface of WS_2, it acted as an optical absorption layer. This layer played a crucial role in enhancing the absorption of UV light with shorter wavelengths and reducing the reflection of visible light with longer wavelengths.[38,39] As a result, the photoelectric conversion capability of WS_2 PDs was improve.

Similarly, we conducted a universal study on enhancement of photoelectric performance of TMDs through Lewis acid doping in the ultraviolet region. As shown in Fig. S7, the absorption of 365 nm light was enhanced after doping MoS_2, $MoSe_2$, and WSe_2, demonstrating that Lewis acid doping has a certain degree of universality in enhancing the light absorption of TMDs in the ultraviolet region.

Table 1. Summary of photodetection performance parameters for TMDs-based PDs.

Material	λ (nm)	$T_{\text{rise}}/T_{\text{fall}}$ (ms)	R (mA/W)	D^* (Jones)	EQE (100%)	References
$SnCl_4/WS_2$	365	24/20	664	3.32×10^{11}	226%	this work
$FePS_3/WS_2$	405	220/160	32.5	1.73×10^{12}	78.4%	[30]
WS_2/Gr	390	2200/3100	439	1.41×10^{10}	81.39%	[31]
Gr/$MoSe_2$	450	9.6/12.8	89.5	2.24×10^{10}	–	[32]
MoS_2/GNR	390	2000/2000	18.81	4.65×10^{8}	19.91%	[33]
MoO_3/MoS_2	425	600/600	160	2.8×10^{11}	55%	[34]
$MoTe_2/MoS_2$	473	285/453	64	1.6×10^{10}	–	[35]
ZnO/MoS_2	405	1510/1100	84	1.05×10^{11}	25.7%	[36]

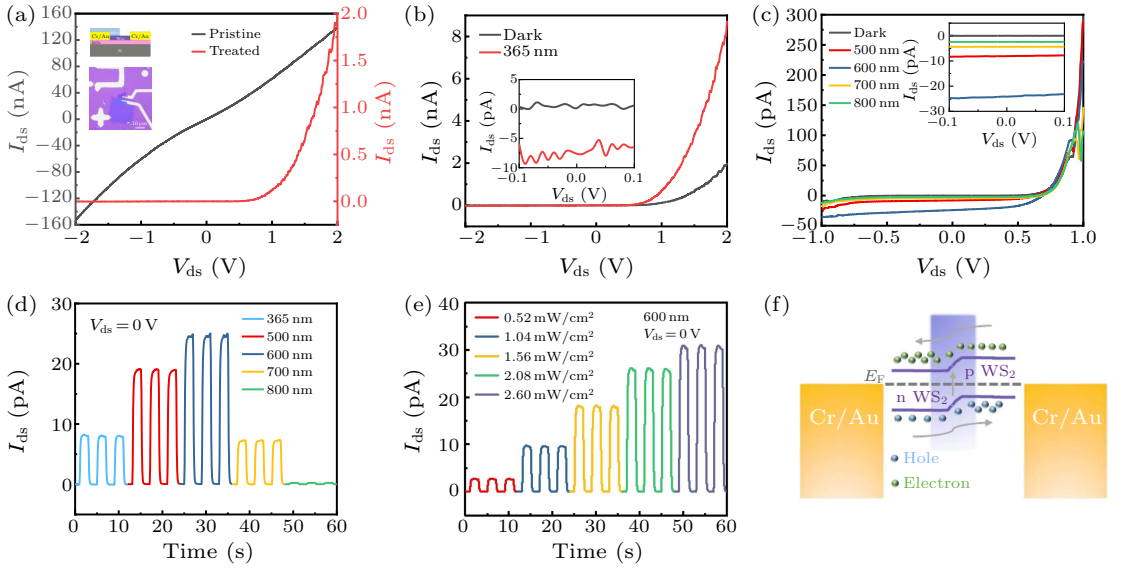


Fig. 5. (a) Output characteristic curves of WS_2 before and after spatial selective doping, with insets showing the WS_2 lateral p–n junction structural schematic diagram (top) and optical microscopy image (bottom). [(b), (c)] I–V curves of p–n junctions under dark conditions and laser irradiation, with insets showing the magnified views near zero bias. (d) Photoresponse of p–n junctions at different laser wavelengths, $V_{ds} = 0$ V. (e) Photoresponse of p–n junctions at different laser power densities (600 nm), $V_{ds} = 0$ V. (f) Energy band diagram of a WS_2 homogeneous p–n junction under illumination.

In addition, we fabricated a WS_2 lateral p–n homojunction through spatial selective doping. By utilizing electron beam lithography (EBL) and atomic layer deposition (ALD), a transparent HfO_2 layer was deposited on one half of the WS_2 channel to prevent p-type doping by $SnCl_4$. The other half remained exposed and could be doped in a $SnCl_4$ solution, as depicted in the inset in Fig. 5(a). Before doping, the output characteristic curve was symmetric about the origin, indicating good ohmic contact. After doping, the device exhibited a rectification ratio of approximately 10^3. Moreover, the photovoltaic effect can be observed as shown in the insets in Figs. 5(b) and 5(c), confirming the successful construction of a WS_2 lateral p–n homojunction.

Therefore, we investigated the photoresponse of WS_2 PDs at zero bias. WS_2 homogeneous p–n junction PDs exhibit rapid photoresponse under 365 nm, 500 nm, 600 nm, and 700 nm lasers [Fig. 5(d)]. The photocurrent increases with power density [Fig. 5(e)], which demonstrates the self-driven effect of WS_2 lateral p–n homojunction PDs. The photovoltaic mechanism could be explained by the energy band diagram shown in Fig. 5(f). When photons were incident on the surface of WS_2, electrons in the valence band were excited to the conduction band, generating electron-hole pairs. The built-in electric field within the p–n junction rapidly separated these electron-hole pairs, resulting in a photocurrent even without a bias voltage.

4. Conclusion

In summary, we have achieved effective p-type doping of WS_2 by immersing TMDs in a $SnCl_4$ ethanol solution. This doping method is simple to perform, causes minimal damage to the crystal structure, and enables precise control of the doping effect by adjusting the temperature, concentration, and duration of the doping process. The Lewis acid $SnCl_4$ not only serves as a p-type dopant but also acts as a light absorber, significantly enhancing the photoelectric performance of the devices in the UV region. At the same time, the UV-to-visible photoconversion capability of Sn doped WS_2 was also improved. Moreover, the p-type doping technique was applied to other types of TMDs, including MoS_2, $MoSe_2$, and WSe_2, resulting in successful p-type doping and improved UV photoconversion capabilities. These findings not only confirm the universality of the proposed doping method but also provide new insights into the potential application of TMDs in the field of UV photodetectors.

Acknowledgments

This work was financially supported by the National Natural Science Foundation of China (Grant Nos. 12025503, U23B2072, 12074293, and 12275198) and the Fundamental Research Funds for the Center Universities (Grant Nos. 2042024kf0001 and 2042023kf0196).

References

[1] Zhang Q Y, Li N, Zhang T, Dong D M, Yang Y T, Wang Y H, Dong Z A, Shen J Y, Zhou T H, Liang Y L, Tang W H, Wu Z P, Zhang Y and Hao J H 2023 *Nat. Commun.* **14** 418
[2] Guo L, Guo Y A, Wang J X and Wei T B 2021 *J. Semicond.* **42** 081801
[3] Raeiszadeh M and Adeli B 2020 *ACS Photon.* **7** 2941
[4] Wang X L, Chen Y F, Liu F and Pan Z W 2020 *Nat. Commun.* **11** 2040
[5] Ouyang W X, Chen J X, Shi Z F and Fang X S 2021 *Appl. Phys. Rev.* **8** 031315
[6] Um D Y, Chandran B, Kim J Y, Oh J K, Kim S U, An J U, Lee C R and Ra Y H 2023 *Adv. Funct. Mater.* **33** 2306143
[7] Wang J J, Fu C, Cheng H Y, Tong X W, Zhang Z X, Wu D, Chen L M, Liang F X and Luo L B 2021 *ASC Nano* **15** 16729
[8] Gong C H, Chu J W, Yin C J, Yan C Y, Hu X Z, Qian S F, Hu Y, Hu K, Huang J W, Wang H B, Wang Y, Wangyang P H, Lei T Y, Dai L P, Wu C Y, Chen B, Li C B, Liao M, Zhai T Y and Xiong J 2019 *Adv. Mater.* **31** 1903580
[9] Tang X, Li K H, Zhao Y, Sui Y, Liang H L, Liu Z, Liao C H, Babatain W, Lin R Y, Wang C J, Lu Y, Alqatari F S, Mei Z X, Tang W H and Li X H 2022 *ACS Appl. Mater. Inter.* **14** 1304
[10] Bu T, Duan X P, Liu C, Su W H, Hong X T, Hong R H, Zhou X J, Liu Y, Fan Z Y, Zou X M, Liao L and Liu X Q 2023 *Adv. Funct. Mater.* **33** 2305490
[11] Wang B H, Xing Y H, Dong S Y, Li J H, Han J, Tu H Y, Lei T, He W X, Zhang B S and Zeng Z M 2023 *Chin. Phys. B* **32** 098504
[12] Li C L, Cao Q, Wang F Z, Xiao Y Q, Li Y B, Delaunay J J and Zhu H W 2018 *Chem. Soc. Rev.* **13** 4981
[13] Manzeli S, Ovchinnikov D, Pasquier D, Yazyev O V and Kis A 2017 *Nat. Rev. Mater.* **2** 17033
[14] Li G, Chen M Q, Zhao S X, Li P W, Hu J, Sang S B and Hou J J 2016 *Acta Phys.-Chim. Sin.* **32** 2905
[15] Wu W B, Ruan Z H, Li J Z, Li Y D, Jiang Y Q, Xu X Z, Li D F, Yuan Y and Lin K F 2019 *Nano-Micro Lett.* **11** 10
[16] Luo Y T, Zhang S Q, Pan H Y, Xiao S J, Guo Z L, Tang L, Khan U, Ding B F, Li M, Cai Z Y, Zhao Y, Lv W, Feng Q L, Zou X L, Lin J H, Cheng H M and Liu B L 2020 *ACS Nano* **14** 767
[17] Wang J, He D, Chen R, Xu H, Wang H B, Yang M H, Zhang Q, Jiang C Z, Li W Q, Ouyang X P and Xiao X H 2023 *InfoMat* **5** e12476
[18] Nagaoka A, Kimura K, Ang A K R, Takabayashi Y, Yoshino K, Sun Q D, Dou B Y, Wei S H, Hayashi K and Nishioka K 2023 *J. Am. Chem. Soc.* **16** 9191
[19] Torsi R, Munson K T, Pendurthi R, Marques E, Van Troeye B, Huberich L, Schuler B, Feidler M, Wang K, Pourtois G, Das S, Asbury J B, Lin Y C and Robinson J A 2023 *ACS Nano* **16** 15629
[20] Kim J K, Cho K, Jang J, Baek K Y, Kim J, Seo J, Song M W, Shin J, Kim J, Parkin S S P, Lee J H, Kang K H and Lee T 2021 *Adv. Mater.* **33** 2101598
[21] Pan X, Zheng Y, Shi Y M and Chen W 2021 *ACS Mater. Lett.* **3** 235
[22] Maity S, Sarkar K and Kumar P 2023 *Nanoscale* **15** 16068
[23] Bar-Saden M and Tenne R 2024 *Nat. Mater.* **23** 310
[24] Peimyoo N, Yang W H, Shang J Z, Shen X N, Wang Y L and Yu T 2014 *ACS Nano* **11** 11320
[25] Jeong I, Cho K, Yun S, Shin J, Kim J, Kim G T, Lee T and Chung S 2022 *ACS Nano* **16** 6215
[26] Zhu Q, Li W H, Wu J X, Tian N C, Li Y W, Yang J W and Liu B T 2022 *ACS Appl. Mater. Inter.* **14** 51994
[27] Bussolotti F, Kawai H, Maddumapatabandi T D, Fu W, Khoo K H, Goh and K E J 2024 *ACS Nano* **18** 8706
[28] Li Z X, Li D Y, Wang H Y, Xu X, Pi L J, Chen P, Zhai T Y and Zhou X 2022 *ACS Nano* **16** 4884
[29] Yang J L, Liu Y, Wang E Y, Pang J B, Huang S R, Gemming T, Bi J S, Bachmatiuk A, Jia H, Hu S X, Jiang C Y, Liu H, Cuniberti G, Zhou W J and Rümmeli M H 2023 *Nano Res.* **17** 3232
[30] Cao X Y, Yan S H, Li Z T, Fang Z H, Wang L, Liu X F, Chen Z W, Lei H C and Zhang X 2023 *J. Phys. Chem. Lett.* **14** 11529
[31] Pataniya P M and Sumesh C K 2020 *ACS Appl. Nano Mater.* **3** 6935
[32] Liu B Y, Zhao C, Chen X Q, Zhang L R, Li Y F, Yan H and Zhang Y Z 2019 *Superlattice Microst.* **130** 87

[33] Rahman S, Tabassum R and Hafiz A K 2024 *Opt. Laser. Technol.* **172** 110494
[34] Pal S, Mukherjee S, Nand M, Srivastava H, Mukherjee C, Jha S N and Ray S K 2020 *Appl. Surf. Sci.* **502** 144196
[35] Wang F, Yin L, Wang Z X, Xu K, Wang F M, Shifa T A, Huang Y, Jiang C and He J 2016 *Adv. Funct. Mater.* **26** 5499
[36] Zhou Y H, Zhang Z B, Xu P, Zhang H and Wang B 2019 *Nanoscale Res. Lett.* **14** 364
[37] Lei S D, Wang X F, Li B, Kang J H, He Y M, George A, Ge L H, Gong Y J, Dong P, Jin Z H, Brunetto G, Chen W B, Lin Z T, Baines R, Galvao D S, Lou J, Barrera E, Banerjee K, Vajtai R and Ajayan P 2016 *Nat. Nanotechnol.* **11** 465
[38] Wu C Y, Zeng B, Zhou K N, Shan L Q, Wang J J, Wang L, Yang Y Z, Zhou Y X and Luo L B 2022 *IEEE Trans. Electron. Dev.* **69** 2469
[39] Li S P, Lei T, Yan Z X, Wang Y, Zhang L K, Tu H Y, Shi W H and Zeng Z M 2024 *Chin. Phys. B* **33** 018501